combinations of clusters is displayed at the same time, without any selection of an arbitrary threshold.

4) Threshold for evaluating the relationships with other known gene information. Although only overlap blocks with 2.0 or higher evaluation values for the representation of genes with putative transcription factor binding sites were color coded in Fig. 4*E* and Fig. 4*F*, users can interactively change this value.

Conclusion

In this report we described the characteristics of the CODM method, a visualization tool for comparing clustering results of gene expression profiles under two different conditions. In CODM, the utilization of 3D space and color allows us to intuitively visualize changes in the composition of cluster sets, changes in the expression patterns of genes between the two conditions, and the relationships with a known gene classification such as transcription factors. Comparison of dynamic changes of gene expression levels across time under different conditions is required in a wide variety of fields of gene expression analysis, including toxicogenomics and pharmacogenomics. Since CODM integrates and simultaneously visualizes various types of information across clustering results, it can be applied to various analyses in these fields.

APPENDIX

Similarity f(T,S)

$$f(T,S) = 1 - \frac{1}{N_{TS}} \sum_{k=1}^{N_{TS}} \sum_{i=1}^{12} (x_{ki} - y_{ki})^2$$

$$= 1 - \frac{1}{N_{TS}} \sum_{k=1}^{N_{TS}} \left\{ \sum_{i=1}^{12} (x_{ki}^2 + y_{ki}^2) - \sum_{i=1}^{12} 2x_{ki}y_{ki} \right\}$$

$$= 1 - \frac{1}{N_{TS}} \sum_{k=1}^{N_{TS}} \left\{ 1 - \sum_{i=1}^{12} 2x_{ki}y_{ki} \right\} \left(\because \sum_{i}^{12} (x_i^2 + y_i^2) = 1 \right)$$

$$= \frac{1}{N_{TS}} \sum_{k=1}^{N_{TS}} \sum_{i=1}^{12} 2x_{ki}y_{ki}$$

The similarity $f(T, S)$ satisfies the following inequality:

$$-1 \le f(T,S) \le 1$$

Proof. Since $f(T,S) \le 1$ is obvious, we only need to prove $-1 \le f(T,S)$. We begin by showing that

$$g = \sum_{i=1}^{12} 2x_i y_i \ge -1$$

where

$$\sum_{i}^{12} (x_i^2 + y_i^2) = 1$$

We consider the Lagrangian function

$$L = \sum_{i=1}^{12} 2x_i y_i + \gamma \left\{ \sum_{i}^{12} (x_i^2 + y_i^2) - 1 \right\}$$

where γ is a Lagrange undetermined multiplier. By taking the derivative, we convert the constrained optimization problem into an unconstrained problem as follows:

$$\frac{\partial L}{\partial x_i} = 2y_i + 2\gamma x_i = 0 \quad (i = 1 \ldots 12)$$

$$\frac{\partial L}{\partial y_i} = 2x_i + 2\gamma y_i = 0 \quad (i = 1 \ldots 12)$$

$$\frac{\partial L}{\partial \gamma} = \sum_{i}^{12} (x_i^2 + y_i^2) - 1 = 0$$

The solutions of this problem are

$x_i = y_i \quad (i = 1,2,\ldots,12), \quad \gamma = -1 \Rightarrow g$ has maximum value 1

or

$x_i = -y_i \quad (i = 1,2,\ldots,12), \quad \gamma = 1 \Rightarrow g$ has the minimum value -1

Therefore,

$$f(T,S) = \frac{1}{N_{TS}} \sum_{k=1}^{N_{TS}} \sum_{i=1}^{12} 2x_{ki}y_{ki} \ge \frac{1}{N_{TS}} \sum_{k=1}^{N_{TS}} (-1) = -1$$

REFERENCES

1. **Alizadeh AA and Staudt LM.** Genomic-scale gene expression profiling of normal and malignant immune cells. *Curr Opin Immunol* 12: 219–225, 2000.
2. **Chiang LW, Grenier JM, Ettwiller L, Jenkins LP, Ficenec D, Martin J, Jin F, DiStefano PS, and Wood A.** An orchestrated gene expression component of neuronal programmed cell death revealed by cDNA array analysis. *Proc Natl Acad Sci USA* 98: 2814–2819, 2001.
3. **Cho RJ, Huang M, Campbell MJ, Dong H, Steinmetz L, Sapinoso L, Hampton G, Elledge SJ, Davis RW, and Lockhart DJ.** Transcriptional regulation and function during the human cell cycle. *Nat Genet* 27: 48–54, 2001.
4. **Eisen MB, Spellman PT, Brown PO, and Botstein D.** Cluster analysis and display of genome-wide expression patterns. *Proc Natl Acad Sci USA* 95: 14863–14868, 1998.
5. **Huang LE, Arany Z, Livingston DM, and Bunn HF.** Activation of hypoxia-inducible transcription factor depends primarily upon redox-sensitive stabilization of its alpha subunit. *J Biol Chem* 271: 32253–32259, 1996.
6. **Ishii M, Hashimoto S, Tsutsumi S, Wada Y, Matsushima K, Kodama T, and Aburatani H.** Direct comparison of GeneChip and SAGE on the quantitative accuracy in transcript profiling analysis. *Genomics* 68: 136–143, 2000.
7. **Kano M, Nishimura K, Tsutsumi S, Aburatani H, Hirota K, and Hirose M.** Cluster overlap distribution map: visualization for gene expression analysis using immersive projection technology. *Presence: Teleoperators and Virtual Environments* 12: 96–109, 2003.
8. **Kawahara N, Wang Y, Mukasa A, Furuya K, Shimizu T, Hamakubo T, Aburatani H, Kodama T, and Kirino T.** Genome-wide gene expression analysis for induced ischemic tolerance and delayed neuronal death following transient global ischemia in rats. *J Cereb Blood Flow Metab* 24: 212–223, 2004.
9. **Kirino T.** Ischemic tolerance. *J Cereb Blood Flow Metab* 22: 1283–1296, 2002.
10. **Manger ID and Relman DA.** How the host "sees" pathogens: global gene expression responses to infection. *Curr Opin Immunol* 12: 215–218, 2000.
11. **Matys V, Fricke E, Geffers R, Gossling E, Haubrock M, Hehl R, Hornischer K, Karas D, Kel AE, Kel-Margoulis OV, Kloos DU, Land S, Lewicki-Potapov B, Michael H, Munch R, Reuter I, Rotert S, Saxel**

H, Scheer M, Thiele S, and Wingender E. TRANSFAC: transcriptional regulation, from patterns to profiles. *Nucleic Acids Res* 31: 374–378, 2003.
12. **Rhodes DR, Barrette TR, Rubin MA, Ghosh D, and Chinnaiyan AM.** Meta-analysis of microarrays: interstudy validation of gene expression profiles reveals pathway dysregulation in prostate cancer. *Cancer Res* 62: 4427–4433, 2002.
13. **Saban MR, Hellmich H, Nguyen NB, Winston J, Hammond TG, and Saban R.** Time course of LPS-induced gene expression in a mouse model of genitourinary inflammation. *Physiol Genomics* 5: 147–160, 2001.
14. **Seo J and Shneiderman B.** Interactively exploring hierarchical clustering results. *IEEE Computer* 35: 80–86, 2002.
15. **Shiffman D, Mikita T, Tai JT, Wade DP, Porter JG, Seilhamer JJ, Somogyi R, Liang S, and Lawn RM.** Large scale gene expression analysis of cholesterol-loaded macrophages. *J Biol Chem* 275: 37324–37332, 2000.
16. **Tamayo P, Slonim D, Mesirov J, Zhu Q, Kitareewan S, Dmitrovsky E, Lander ES, and Golub TR.** Interpreting patterns of gene expression with self-organizing maps: methods and application to hematopoietic differentiation. *Proc Natl Acad Sci USA* 96: 2907–2912, 1999.
17. **Tavazoie S, Hughes JD, Campbell MJ, Cho RJ, and Church GM.** Systematic determination of genetic network architecture. *Nat Genet* 22: 281–285, 1999.
18. **Wang GL, Jiang BH, Rue EA, and Semenza GL.** Hypoxia-inducible factor 1 is a basic-helix-loop-helix-PAS heterodimer regulated by cellular O_2 tension. *Proc Natl Acad Sci USA* 92: 5510–5514, 1995.
19. **Yan SF, Lu J, Zou YS, Soh-Won J, Cohen DM, Buttrick PM, Cooper DR, Steinberg SF, Mackman N, Pinsky DJ, and Stern DM.** Hypoxia-associated induction of early growth response-1 gene expression. *J Biol Chem* 274: 15030–15040, 1999.

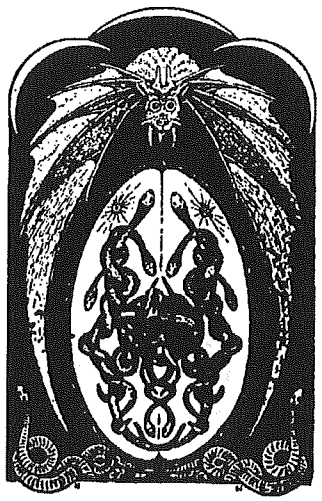

ORIGINAL PAPER

Vol. 21 no. 4 2005, pages 439–444
doi:10.1093/bioinformatics/bti188

Multidimensional support vector machines for visualization of gene expression data

D. Komura [1,*], H. Nakamura[1], S. Tsutsumi[1], H. Aburatani[2] and S. Ihara[1]

[1]Research Center for Advanced Science and Technology and [2]Genome Science Division, Center for Collaborative Research, University of Tokyo, Tokyo 153-8904, Japan

Received on May 21, 2004; accepted on November 11, 2004
Advance Access publication December 17, 2004

ABSTRACT

Motivation: Since DNA microarray experiments provide us with huge amount of gene expression data, they should be analyzed with statistical methods to extract the meanings of experimental results. Some dimensionality reduction methods such as Principal Component Analysis (PCA) are used to roughly visualize the distribution of high dimensional gene expression data. However, in the case of binary classification of gene expression data, PCA does not utilize class information when choosing axes. Thus clearly separable data in the original space may not be so in the reduced space used in PCA.

Results: For visualization and class prediction of gene expression data, we have developed a new SVM-based method called multidimensional SVMs, that generate multiple orthogonal axes. This method projects high dimensional data into lower dimensional space to exhibit properties of the data clearly and to visualize a distribution of the data roughly. Furthermore, the multiple axes can be used for class prediction. The basic properties of conventional SVMs are retained in our method: solutions of mathematical programming are sparse, and nonlinear classification is implemented implicitly through the use of kernel functions. The application of our method to the experimentally obtained gene expression datasets for patients' samples indicates that our algorithm is efficient and useful for visualization and class prediction.

Contact: komura@hal.rcast.u-tokyo.ac.jp

1 INTRODUCTION

DNA microarray has been the key technology in modern biology and helped us to decipher the biological system because of its ability to monitor the expression levels of thousands of genes simultaneously. Since DNA microarray experiments provide us with huge amount of gene expression data, they should be analyzed with statistical methods to extract the meanings of experimental results.

A great number of supervised learning algorithms have been proposed and applied to classification of gene expression data (Golub *et al.*, 1999; Tibshirani *et al.*, 2002; Khan *et al.*, 2001). Support Vector Machines (SVMs) have been paid attention in recent years because of their good performance in various fields, especially in the area of bioinformatics including classification of gene expression data (Furey *et al.*, 2000). However, SVMs predict a class of test samples by projecting the data into one-dimensional space based on a decision function. As a result, information loss of the original data is enormous.

Some methods are used for projecting high dimensional data into lower dimensional space to clearly exhibit the properties of the data and to roughly visualize the distribution of the data. Principal Component Analysis (PCA) (Fukunaga, 1990) and its derivatives, e.g. Nonlinear PCA (Diamantaras and Kung, 1996) and Kernel PCA (Schölkopf *et al.*, 1998), are most widely used for this purpose (Huang *et al.*, 2003). One drawback of PCA analysis is, however, that class information is not utilized for class prediction because PCA chooses axes based on the variance of overall data. Thus clearly separable data in the original space may not be so in the reduced space used in PCA. Another method for visualization and reducing dimension of data is discriminant analysis. It chooses axes based on class information in terms of within- and between-class variance. However, it is reported that SVMs often outperform discriminant analysis (Brown *et al.*, 2000).

The main purpose of this paper is to cover the shortcoming of SVMs by introducing multiple orthogonal axes for reducing dimensions and visualization of gene expression data. To this end, we have developed multidimensional SVMs (MD-SVMs), a new SVM-based method that generates multiple orthogonal axes based on margin between two

*To whom correspondence should be addressed.

Komura *et al.* (2004) Multidimensional Support Vector Machines for Visualization of Gene Expression Data. Symposium on Applied Computing, Proceedings of the 2004 ACM symposium on Applied computing, 175-179; http://doi.acm.org/10.1145/967900.967936

classes to minimize generalization errors. The axes generated by this method reduce dimensions of original data to extract information useful in estimating the discriminability of two classes. This method fulfills the requirement of both visualization and class prediction. The basic properties of SVMs are retained in our method: solutions of mathematical programming are sparse, and nonlinear classification of data is implemented implicitly through the use of kernel functions.

This paper is organized as follows. In Section 2, we introduce the fundamental of SVMs. In Section 3, we describe the algorithm of MD-SVMs. In Section 4 and 5, we show numerical experiments on real gene expression datasets and reveal that our algorithm is effective for data visualization and class prediction.

1.1 Notation

$\mathbb{R}$ is defined as the set of real numbers. Each component of a vector $\boldsymbol{x} \in \mathbb{R}^n, i = 1,\ldots,m$ will be denoted by $x_j, j = 1,\ldots,n$. The inner product of two vectors $\boldsymbol{x} \in \mathbb{R}^n$ and $\boldsymbol{y} \in \mathbb{R}^n$ will be denoted by $\boldsymbol{x} \cdot \boldsymbol{y}$. For a vector $\boldsymbol{x} \in \mathbb{R}^n$ and a scalar $a \in \mathbb{R}, a \leq \boldsymbol{x}$ is defined as $a \leq x_i$ for all $i = 1,\ldots,n$. For an arbitrary variable x, x^k is just a name of the variable with upper suffix, not defined as k-th power of x.

2 SUPPORT VECTOR MACHINES

Since details of SVMs are fully described in the articles (Vapnik, 1998; Cristianini and Shawe-Taylor, 2000), we briefly introduce the fundamental principle of SVMs in this section. We consider a binary classification problem, where a linear decision function is employed to separate two classes of data based on m training samples $\boldsymbol{x}_i \in \mathbb{R}^n, i = 1,\ldots,m$ with corresponding class values $y_i \in \{\pm 1\}, i = 1,\ldots,m$. SVMs map a data $\boldsymbol{x} \in \mathbb{R}^n$ into a higher, probably infinite, dimensional space $\mathbb{R}^N$ than the original space with an appropriate nonlinear mapping $\phi : \mathbb{R}^n \to \mathbb{R}^N, n < N$. They generate the linear decision function of the form $f(\boldsymbol{x}) = \mathrm{sign}(\boldsymbol{w} \cdot \phi(\boldsymbol{x}) + b)$ in the high dimensional space, where $\boldsymbol{w} \in \mathbb{R}^N$ is a weight vector which defines a direction perpendicular to the hyperplane of the decision function, while $b \in \mathbb{R}$ is a bias which moves the hyperplane parallel to itself. The optimal decision function given by SVMs is a solution of an optimization problem

$$\min_{w,\xi} \frac{1}{2}\|\boldsymbol{w}\|^2 + C\sum_{i=1}^{m}\xi_i,$$

$$\text{s.t. } y_i(\boldsymbol{w} \cdot \phi(\boldsymbol{x}_i) + b) \geq 1 - \xi_i, \quad i = 1,\ldots,m, \ \boldsymbol{\xi} \geq 0, \quad (1)$$

with $C > 0$. Here, $\boldsymbol{\xi} \in \mathbb{R}^m$ is a vector whose elements are slack variables and $C \in \mathbb{R}$ is a regularization parameter for penalizing training errors. When $C \to \infty$, no training errors are allowed, and thus this is called hard margin classification. When $0 < C < \infty$, this is called soft margin classification because it allows some training errors. Note that a geometric margin γ between two classes is defined as $\frac{1}{\|w\|^2}$. The optimization problem formalizes the tradeoff between maximizing margin and minimizing training errors. The problem is transformed into its corresponding dual problem by introducing lagrange multiplier $\boldsymbol{\alpha} \in \mathbb{R}^m$ and replacing $\phi(\boldsymbol{x}_i) \cdot \phi(\boldsymbol{x}_j)$ by kernel function $K(\boldsymbol{x}_i, \boldsymbol{x}_j) = \phi(\boldsymbol{x}_i) \cdot \phi(\boldsymbol{x}_j)$ to be solved in an elegant way of dealing with a high dimensional vector space. The dual problem is

$$\max_{\alpha} -\frac{1}{2}\sum_{i=1}^{m}\sum_{j=1}^{m}\alpha_i\alpha_j y_i y_j K(\boldsymbol{x}_i, \boldsymbol{x}_j) + \sum_{i=1}^{m}\alpha_i,$$

$$\text{s.t. } 0 \leq \boldsymbol{\alpha} \leq C, \sum_{i=1}^{m}\alpha_i y_i = 0. \quad (2)$$

By virtue of the kernel function, the value of the inner product $\phi(\boldsymbol{x}_i) \cdot \phi(\boldsymbol{x}_j)$ can be obtained without explicit calculation of $\phi(\boldsymbol{x}_i)$ and $\phi(\boldsymbol{x}_j)$. Finally, the decision function becomes $f(\boldsymbol{x}) = \mathrm{sign}\left(\sum_{i=1}^{m}\alpha_i y_i K(\boldsymbol{x}_i, \boldsymbol{x}) + b\right)$. by using kernel functions between training samples $\boldsymbol{x}_i, i = 1,\ldots,m$ and a test sample $\boldsymbol{x}$.

3 MULTIDIMENSIONAL SUPPORT VECTOR MACHINES

In order to overcome the drawback that SVMs cannot generate more than one decision function, we propose a SVM-based method that can be used for both data visualization and class prediction in this section. We call this method multidimensional SVMs (MD-SVMs). We deal with the same problem as mentioned in Section 2. Conventional SVMs give an optimal solution set $(\boldsymbol{w}, b, \boldsymbol{\xi})$ which corresponds to a decision function, while our MD-SVMs give the multiple sets $(\boldsymbol{w}^k, b^k, \boldsymbol{\xi}^k), k = 1,2,\ldots,l$ with $l \leq n$, so that all the directions $\boldsymbol{w}_k$ are orthogonal to one another. The orthogonal axes can be used for reducing the dimension of original data and data visualization in three dimensional space by means of projection. Here the first set $(\boldsymbol{w}^1, b^1, \boldsymbol{\xi}^1)$ is equivalent to that obtained by conventional SVMs. Now we only refer to the steps of obtaining $(\boldsymbol{w}^k, b^k, \boldsymbol{\xi}^k), k = 2,3,\ldots,l$. In practice, the k-th set $(\boldsymbol{w}^k, b^k, \boldsymbol{\xi}^k) k = 2,3,\ldots,l$ are found with iterative computations of the optimization problem

$$\min_{\boldsymbol{w}^k,\boldsymbol{\xi}^k} \frac{1}{2}\|\boldsymbol{w}^k\|^2 + C\sum_{i=1}^{m}\xi_i^k,$$

$$\text{s.t. } y_i(\boldsymbol{w}^k \cdot \phi(\boldsymbol{x}_i) + b^k) \geq 1 - \xi_i^k, i = 1,\ldots,m,$$

$$\boldsymbol{\xi}^k \geq 0, \boldsymbol{w}^k \cdot \boldsymbol{w}^j = 0, j = 1,\ldots,k-1. \quad (3)$$

This problem differs from that of conventional SVMs in the last constraint $\boldsymbol{w}^k \cdot \boldsymbol{w}^j = 0$. The weight vector $\boldsymbol{w}^j, j = 1,\ldots,k-1$ should be computed in advance by solving

other optimization problems (3). The optimization problem is modified by introducing lagrange multipliers $\alpha^k, \gamma^k \in \mathbb{R}^m$, $\beta^k \in \mathbb{R}^{k-1}$ and kernel functions. The primal Lagrangian is

$$L(w^k, b^k, \xi^k) = \frac{1}{2}\| w^k \|^2 + C\sum_{i=1}^{m}\xi_i^k + \sum_{i=1}^{m}\alpha_i^k(1 - \xi_i^k - y_i(w^k \cdot \phi(x_i) + b^k)) + \sum_{j=1}^{k-1}\beta_j^k(w^k \cdot w^j) - \sum_{i=1}^{m}\gamma_i^k\xi_i. \quad (4)$$

Consequently, the optimization problem is

$$\max_{\alpha^k,\beta^k} -\frac{1}{2}\sum_{i=1}^{m}\sum_{j=1}^{m}\alpha_i^k\alpha_j^k y_i y_j K(x_i, x_j) + \frac{1}{2}\sum_{i=1}^{k-1}\beta_i^k\beta_i^k(w^i \cdot w^i) + \sum_{i=1}^{m}\alpha_i^k,$$

$$\text{s.t. } 0 \le \alpha^k \le C, \sum_{i=1}^{m}\alpha_i^k y_i = 0,$$

$$\sum_{i=1}^{m}\alpha_i^k y_i(\phi(x_i) \cdot w^j) = 0, j = 1, \ldots, k-1 \quad (5)$$

Here $\phi(x_p) \cdot w^q$ and $w^p \cdot w^p$ are calculated recursively as follows:

$$\phi(x_p) \cdot w^q = \sum_{i=1}^{m}\alpha_i^q y_i K(x_p, x_i) - \sum_{i=1}^{q-1}\beta_i^q(\phi(x_p) \cdot w^i), \quad (6)$$

$$w^p \cdot w^p = \sum_{i=1}^{m}\sum_{j=1}^{m}\alpha_i^p\alpha_j^p y_i y_j K(x_i, x_j) - \sum_{i=1}^{m}\sum_{j=1}^{p-1}\alpha_i^p y_i\beta_j^p(\phi(x_i) \cdot w^j) + \sum_{i=1}^{p-1}\beta_i^p\beta_i^p(w^i \cdot w^i) - \sum_{i=1}^{m}\sum_{j=1}^{p-1}\alpha_i^p y_i\beta_j^p(\phi(x_i) \cdot w^j), \quad (7)$$

where $\phi(x_p) \cdot w^1 = \sum_{i=1}^{m}\alpha_i^1 y_i K(x_p, x_i)$ and $w^1.w^1 = \sum_{i=1}^{m}\alpha_i^1 y_i(\phi(x_i), w^1)$. As can be seen, there is no need to calculate nonlinear map of data $\phi(x)$ in problem (5) because all nonlinear mappings can be replaced with kernel functions.

Note that this optimization problem is a nonconvex quadratic problem when k is more than 1. As a consequence, the optimal solutions are not easy to be obtained. In Section 4, we use local optimum for numerical experiments when k is 2 or 3. We note the experimental results are still encouraging.

The corresponding Karush–Kuhn–Tucker conditions are

$$\alpha_i^k\{1 - \xi_i^k - y_i(w^k \cdot \phi(x_i) + b^k)\} = 0, \quad (8)$$

$$\xi_i^k(\alpha_i^k - C) = 0, i = 1, \ldots, m. \quad (9)$$

These are exactly the same as conventional SVMs. We highlight the other properties conserved from conventional SVMs:

- Projecting data into high dimensional space is implicit, using kernel functions to replace inner products.
- The solutions α^k of the optimization problem is sparse. Then the corresponding decision function depends only on few 'Support Vectors'.

Since each decision function is normalized independently to hold $w^k \cdot \phi(x_i) + b^k = y_i$ for $i = 1, \ldots, m$, data scales of the axes should be aligned with first axis ($k = 1$) for visualization. The margin γ^k, the L2-distance between support vectors of each class of k-th axis, is

$$\left(\sum_{i=1}^{m}\sum_{j=1}^{m}\alpha_i^k\alpha_j^k y_i y_j K(x_i, x_j) - \sum_{i=1}^{k-1}\beta_i^k\beta_i^k(w^i \cdot w^i)\right)^{-\frac{1}{2}}. \quad (10)$$

So a scaling factor $s^k = \gamma^1/\gamma^k$ is

$$\sqrt{\frac{\sum_{i=1}^{m}\sum_{j=1}^{m}\alpha_i^1\alpha_j^1 y_i y_j K(x_i, x_j)}{\sum_{i=1}^{m}\sum_{j=1}^{m}\alpha_i^k\alpha_j^k y_i y_j K(x_i, x_j) - \sum_{i=1}^{k-1}\beta_i^k\beta_i^k(w^i \cdot w^i)}}. \quad (11)$$

The decision function of k-th step has the form $f^k(x) = \text{sign}\left(\sum_{i=1}^{m}\alpha_i^k y_i K(x_i, x) + b^k\right)$. Since the right hand side of the equation has the function of projecting original data into one dimensional space, the data can be plot in up to three dimensional space for visualization. The coordinate of data $x \in \mathbb{R}^m$ in three dimensional space is

$$(s^{k_1}g^{k_1}(x), s^{k_2}g^{k_2}(x), s^{k_3}g^{k_3}(x)), \quad (12)$$

where $g^k(x) = \sum_{i=1}^{m}\alpha_i^k y_i K(x_i, x) + b^k$. The space represents a distribution of data clearly based on the margin between two classes.

4 NUMERICAL EXPERIMENTS

4.1 Method

In order to confirm the effectiveness of our algorithm, we have performed numerical experiments. MD-SVMs can generate multiple axes, up to the number of features. Here we choose three axes, $k = 1, 2, 3$, to simplify the experiments. When k is

2 or 3, we use local optimum in problem (5) since it is difficult to obtain the global solutions. In our experiments, we carry out hold-out validation because cross-validation changes decision functions every time the dataset is split. Then we compare the results obtained by MD-SVMs with those obtained by PCA.

In the experiments, the expression values for each of the genes are normalized such that the distribution over the samples has a zero mean and unit variance. Before normalization, we discard genes in the dataset with the overall average value less than 0.35. Then we calculate a score $F(x(j)) = |(\mu^+(j)-\mu^-(j))/(\sigma^+(j)+\sigma^-(j))|$, for the remaining genes. Here $\mu^+(j)(\mu^-(j))$ and $\sigma^+(j)(\sigma^-(j))$ denote the mean and standard deviation of the j-th gene of the samples labeled $+1(-1)$, respectively. This score becomes the highest when the corresponding expression levels of the gene differ most in the two classes and have small deviations in each class. We select 100 genes with the highest scores and use them for hold-out validation. These procedures for gene selection are done only for training data for fair experiments.

The regularization parameter C in problem (5) is set to 1000. This value is rather large but finite because we would like to avoid ill-posed problems in a hard margin classification. We choose linear kernel $K(\boldsymbol{x}_i, \boldsymbol{x}_j) = \boldsymbol{x}_i \cdot \boldsymbol{x}_j$ and RBF kernel $K(\boldsymbol{x}_i, \boldsymbol{x}_j) = \exp -\gamma \| \boldsymbol{x}_i - \boldsymbol{x}_j \|^2$ with $\gamma = 0.001$ in the experiments of MD-SVMs.

4.2 Materials

Leukemia dataset (Golub et al., 1999) This gene expression dataset consists of 72 leukemia samples, including 25 acute myeloid leukemia (AML) samples and 47 acute lymphoblastic leukemia (ALL) samples. They are obtained by hybridization on the Affymetrix GeneChip containing probe sets for 7070 genes. Training set contains 20 AML samples and 42 ALL samples. Test set contains 5 AML samples and 5 ALL samples. AML samples are labeled $+1$ and ALL samples are labeled -1.

Lung tissue dataset (Bhattacharjee et al., 2001) This dataset consists of 203 samples from lung tissue, including 16 samples from normal tissue and 187 samples from cancerous tissue, and is obtained by hybridization on the Affymetrix U95A Genechip containing probe sets for 12558 genes. Training set includes 13 samples from normal tissue and 157 samples from cancerous tissue. Test set includes 3 samples from normal tissue and 30 samples from cancerous tissue. Samples from normal tissue are labeled $+1$ and samples from cancerous tissue are labeled -1.

5 RESULTS AND DISCUSSION

The results of numerical experiments are shown in Figure 1, and Tables 1 and 2. The distributions obtained by MD-SVMs on the leukemia dataset and the lung tissues dataset are given in Figure 1-(1) and 1-(3), respectively. Those obtained by PCA are given in Figure 1-(2) and 1-(4), respectively. The number of misclassified samples by MD-SVMs are summarized in Table 1 and 2. In these tables, the class of the samples is predicted based on decision functions $f^k(\boldsymbol{x}), k = 1, 2, 3$, corresponding to each of the three axes.

Figure 1-(1) and 1-(3) illustrate that MD-SVMs are likely to separate the samples of each class in all the three directions. However, as shown in Figure 1-(2) and 1-(4), PCA does not separate the samples in the directions of the 2nd or the 3rd axis. These axes by PCA are dispensable with the objective of visualization for class prediction. In other words, MD-SVMs gather the plots of the samples into the appropriate clusters of each class, while PCA rather scatters them. Furthermore, in the distribution by MD-SVMs for the lung tissues dataset, one sample outlies from correct clusters (indicated by arrows in Figure 1-(3)). Though this sample also seems to be an outlier in the distribution by PCA (also indicated in Figure 1-(4)), the outlier significantly deviates in MD-SVMs. This may arise from the fact that MD-SVMs can separate the samples in all the directions. These observations indicate that MD-SVMs are well suited for visualizing in binary classification problems.

The significant advantage of MD-SVMs over PCA is the ability to predict the classes. MD-SVMs can predict the classes of samples based on the decision functions $f^k(\boldsymbol{x})$ without extra computation, while PCA cannot. The predicted class of a sample should be matched by the all the decision functions in an ideal case. However that does not always occur as seen in Tables 1 and 2. In such cases, the simplest method for prediction is to use only the 1st axis, which corresponds to the decision function generated by conventional SVMs. The idea is supported by the fact that the 1st decision function classifies the samples most correctly in almost all cases in Tables 1 and 2. The more advanced method is weighted voting. Scaling factor or normalized objective values in problem (5) are the candidate of the weight.

Multiple decision functions generated by MD-SVMs are useful for outlier detection. Samples misclassified by multiple decision functions may be mis-labeled or categorized into unknown classes. For example, see the column '3 axes' of test sample of the lung tissues dataset with RBF kernel in Table 2. This sample is misclassified by all decision functions, so we can say that this data contains some experimental error. The hierarchical clustering method also supports our result. These results indicate that MD-SVMs can be used for finding candidates of outliers.

6 CONCLUSION

For both visualization and class prediction of gene expression data, we propose a new method called Multidimensional Support Vector Machines. We formulate the method as a quadratic program and implement the algorithm. This is motivated by the following facts: (1) SVMs perform better than the other classification algorithms, but they generate only one axis for class prediction. (2) PCA chooses multiple

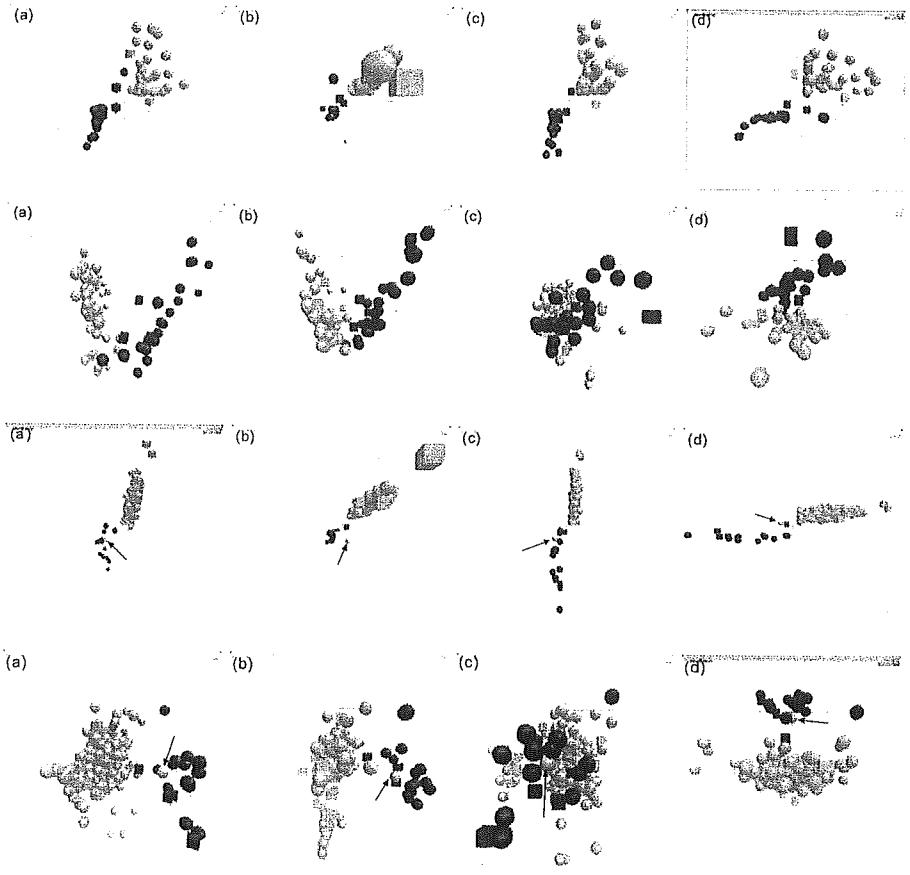

Fig. 1. (Top row) Distribution obtained by MD-SVMs for the leukemia dataset with linear kernel. (Second row) Distribution obtained by PCA on the leukemia dataset. (Third row) Distribution obtained by MD-SVMs for the lung tissues dataset with linear kernel. The sample indicated by arrows appears to be an outlier. (Fourth row) Distribution obtained by PCA for the lung tissues dataset. The sample indicated by arrows is the same as in the third row but with less deviates. (a) Cross shot, (b) 1st axis (x axis) and 2nd axis (y axis), (c) 2nd axis (x axis) and 3rd axis (y axis), (d) 3rd axis (x axis) and 1st axis (y axis). Black objects and white objects indicate AML samples (or normal tissues) ALL samples (or cancreous tissues), respectively. Training data and test data are expressed as a sphere and a cube, respectively.

Table 1. Number of classification errors in the MD-SVMs for the leukemia dataset. The columns 'n-th axis', $n = 1, 2, 3$, indicates the number of samples misclassified by n-th decision function. The columns 'n axes', $n = 1, 2, 3$, indicates the number of samples misclassified by n decision functions

Kernel	Sample	# of samples	1st axis	2nd axis	3rd axis	1 axis	2 axes	3 axes
Linear	Training	62	0	1	2	1	1	0
RBF	Training	62	0	2	7	5	2	0
Linear	Test	10	1	1	2	2	1	0
RBF	Test	10	0	2	0	2	0	0

Table 2. Number of classification errors in the MD-SVMs on the lung dataset. See the caption of Table 1 for other explanation

Kernel	Sample	# of samples	1st axis	2nd axis	3rd axis	1 axis	2 axes	3 axes
Linear	Training	170	0	1	1	0	1	0
RBF	Training	170	0	3	5	2	3	0
Linear	Test	33	1	0	0	1	0	0
RBF	Test	33	1	1	1	0	0	1

orthogonal axes, but it cannot predict classes of samples without other classification algorithms. We have tried to cover the shortcomings of both methods. MD-SVMs choose multiple orthogonal axes, which correspond to decision functions, from high dimensional space based on a margin between two classes. These multiple axes can be used for both visualization and class prediction.

Numerical experiments on real gene expression data indicate the effectiveness of MD-SVMs. All axes generated by MD-SVMs are taken into account for separating class of samples, while the 2nd and the 3rd axes by PCA are not. The samples in the distributions by MD-SVMs gather into appropriate clusters more vividly than those by PCA. MD-SVMs can predict the classes of the samples with multiple decision functions. We also indicate that MD-SVMs are useful for outlier detection with multiple decision functions.

There are several future works to be done on MD-SVMs: (1) application of our method to wider variety of gene expression datasets, (2) investigation of gene selection for preprocess of analysis and (3) investigation on class prediction method with multiple decision functions. Firstly, the use of more suitable samples may show that the axes chosen by MD-SVMs separate samples more clearly than those by PCA. Secondly, since the conventional SVMs show good generalization performance especially with large number of features, it is expected that MD-SVMs show much better performance than PCA with increasing the number of genes used in the numerical experiments. Since the element of weight vector generated by SVMs is one of the measures of discrimination power of the corresponding genes (Guyon *et al.*, 2002), that generated by MD-SVMs can be used for gene selection. Thirdly, the classification with probability as well as the weighted voting mentioned in Section 4 may be achieved in our scheme since the conventional SVMs have been already expanded for the purpose with sigmoid functions (Platt, 1999). We hope that our method sheds some lights on the future study of gene expression experiments.

REFERENCES

Bhattacharjee,A., Richards,W., Staunton,J., Li,C., Monti,S., Vasa,P., Ladd,C., Beheshti,J., Bueno,R., Gillette,M. *et al.* (2001) Classification of human lung carcinomas by mRNA expression profiling reveals distinct adenocarcinoma subclasses. *Proc. Natl Acad. Sci. USA*, **98**, 13790–13795.

Brown,M., Grundy,W., Lin,D., Cristianini,N., Sugnet,C., Furey,T., Ares,M. and Haussler,D. (2000) Knowledge-based analysis of microarray gene expression data by using support vector machines. *Proc. Natl Acad. Sci. USA*, **97**, 262–267.

Cristianini,N. and Shawe-Taylor,J. (2000) *An Introduction to Support Vector Machines and Other Kernel-based Learning Methods.* Cambridge University Press, NY.

Diamantaras,K. and Kung,S. (1996) *Principal Component Neural Networks Theory and Applications.* John Wiley & Sons, NY.

Fukunaga,K. (1990) *Introduction to Statistical Pattern Recognition.* Academic Press, NY.

Furey,T., Cristianini,N., Duffy,N., Bednarski,D., Schummer,M. and Haussler,D. (2000) Support vector machine classification and validation of cancer tissue samples using microarray expression data. *Bioinformatics*, **16**, 906–914.

Golub,T., Slonim,D., Tamayo,P., Huard,C., Gaasenbeek,M., Mesirov,J., Coller,H., Loh,M., Downing,J., Caligiuri,M., Bloomfield,C. and Lander,E. (1999) Molecular classification of cancer: class discovery and class prediction by gene expression monitoring. *Science*, **286**, 531–537.

Guyon,I., Weston,J., Barnhill,S. and Vapnik,V. (2002) Gene selection for cancer classification using support vector machines. *J. Machine Learn.*, **46**, 389–422.

Huang,E., Ishida,S., Pittman,J., Dressman,H., Bild,A., Kloos,M., D'Amico,M., Pestell,R., West,M. and Nevins,J. (2003) Gene expression phenotypic models that predict the activity of oncogenic pathways. *Nat. Genet.*, **34**, 226–230.

Khan,J., Wei,J., Ringnér,M., Saal,L., Ladanyi,M., Westermann,F., Berthold,F., Schwab,M., Antonescu,C., Peterson,C. and Meltzer,P. (2001) Classification and diagnostic prediction of cancers using gene expression profiling and artificial neural networks. *Nat. Med.*, **7**, 673–679.

Platt,J. (1999) *Probabilistic Outputs for Support Vector Machines and Comparisons to Regularized Likelihood Methods.* MIT Press, Cambridge, MA.

Schölkopf,B., Smola,A. and Müller,K. (1998) Non-linear component analysis as a kernel eigenvalue problem. *Neural Comput.*, **10**, 1299–1319.

Tibshirani,R., Hastie,T., Narasimhan,B. and Chu,G. (2002) Diagnosis of multiple cancer types by shrunken centroids of gene expression. *Proc. Natl Acad. Sci. USA*, **99**, 6567–6572.

Vapnik,V. (1998) *Statistical Learning Theory.* John Wiley & Sons, NY.

□ CASE REPORT □

Re-entry Circuit in Ventricular Tachycardia Due to Focal Fatty-fibrosis in a Patient with Myotonic Dystrophy

Hideyuki MURAOKA, Nobuyuki NEGORO, Fumio TERASAKI*, Takahiro NAKAKOJI, Shigeyuki KOJIMA, Masaaki HOSHIGA, Masakazu SUGINO, Takafumi HOSOKAWA, Tadashi ISHIHARA and Toshiaki HANAFUSA

Abstract

A 69-year-old man with a recurrent ventricular tachycardia (VT) was admitted. The patient was diagnosed as myotonic dystrophy type 1 (DM1) and DNA analysis revealed 1,800 CTG-repeat expansion in the myotonic dystrophy protein kinase (DMPK) gene. Ultrasonic cardiogram (UCG), left ventriculogram (LVG) and magnetic resonance imaging (MRI) did not show any abnormal sign including fatty infiltration. But, endomyocardial biopsy obtained from ventricular outflow tract revealed severe fatty infiltration and interstitial fibrosis. Radiofrequency catheter ablation at the biopsy site could eliminate VT, so it was strongly suggested that the re-entry circuit was formed by focal fatty-fibrosis. Careful observation should be continued for a long period.
(Internal Medicine 44: 129–135, 2005)

Key words: myotonic dystrophy, endomyocardial biopsy, fatty-fibrosis, catheter ablation, ventricular tachycardia

Introduction

Myotonic dystrophy type 1 (DM1) is an autosomal dominant disorder, which is caused by the unstable expansion of a CTG trinucleotide repeat located in the 3' untranslated region of the gene encoding DM protein kinase (DMPK) on chromosome 19q13.3 (1–5). DM1 is characterized by myotonia, progressive muscular weakness and atrophy. In addition to its neuromuscular features, there is a broad spectrum of clinical features, such as cataracts, frontal baldness, ptosis, testicular atrophy and various cardiovascular symptoms (6). DM1 is the commonest muscular dystrophy occurring in adult life and cardiac symptoms have been reported in 7 to 23% of these patients (7, 8). Most cardiac events consist of impairment of the cardiac conduction system including bundle branch block or atrioventricular block. These are few reports of ventricular tachycardia (VT), whereas ventricular arrhythmias play a major role in the mortality of these patients (9–13). Unfortunately, pharmacological therapies have not significantly improved the prognosis (14), possibly due to the massive fatty fibrosis in the cardiac muscle. Here, we describe a case of DM1 with ventricular tachycardia caused by re-entry circuit, which was successfully relieved by catheter ablation.

Case Report

A 69-year-old man with a history of recurrent wide QRS tachycardia since December, 2000 was admitted to our hospital for further examination on January 31, 2002. The patient developed gait disturbance over a 10-year period and was diagnosed as having DM1, on the basis of DNA analysis that revealed a heterozygous 1,800 CTG-repeat expansion in the myotonic dystrophy protein kinase (DMPK) gene on chromosome 19q13.3. Two of the patient's brothers and his son were also diagnosed as having DM1. We could not determine whether or not two of the patient's brothers had heart diseases and abnormality in DNA analysis or not, because they had died from suffocation many years ago previously. But his son, who does not have any cardiovascular symptom, has an about 600 CTG-repeat expansion in the DMPK gene in DNA analysis. At the time of the patient's palpitation attack an electrocardiogram (ECG) showed wide QRS tachycardia, which was eliminated spontaneously.

On admission, the patient's blood pressure was 122/76 mmHg, pulse rate was 72 beats/min and regular, and body temperature was 36.0°C. Physical examination revealed frontal baldness, a cataract, ptosis, atrophy of the zygomatic

From the First Department of Internal Medicine and *the Third Department of Internal Medicine, Osaka Medical College, Takatsuki
Received for publication May 10, 2004; Accepted for publication September 21, 2004
Reprint requests should be addressed to Dr. Hideyuki Muraoka, the First Department of Internal Medicine, Osaka Medical College, 2-7 Daigaku-machi, Takatsuki 569-0801

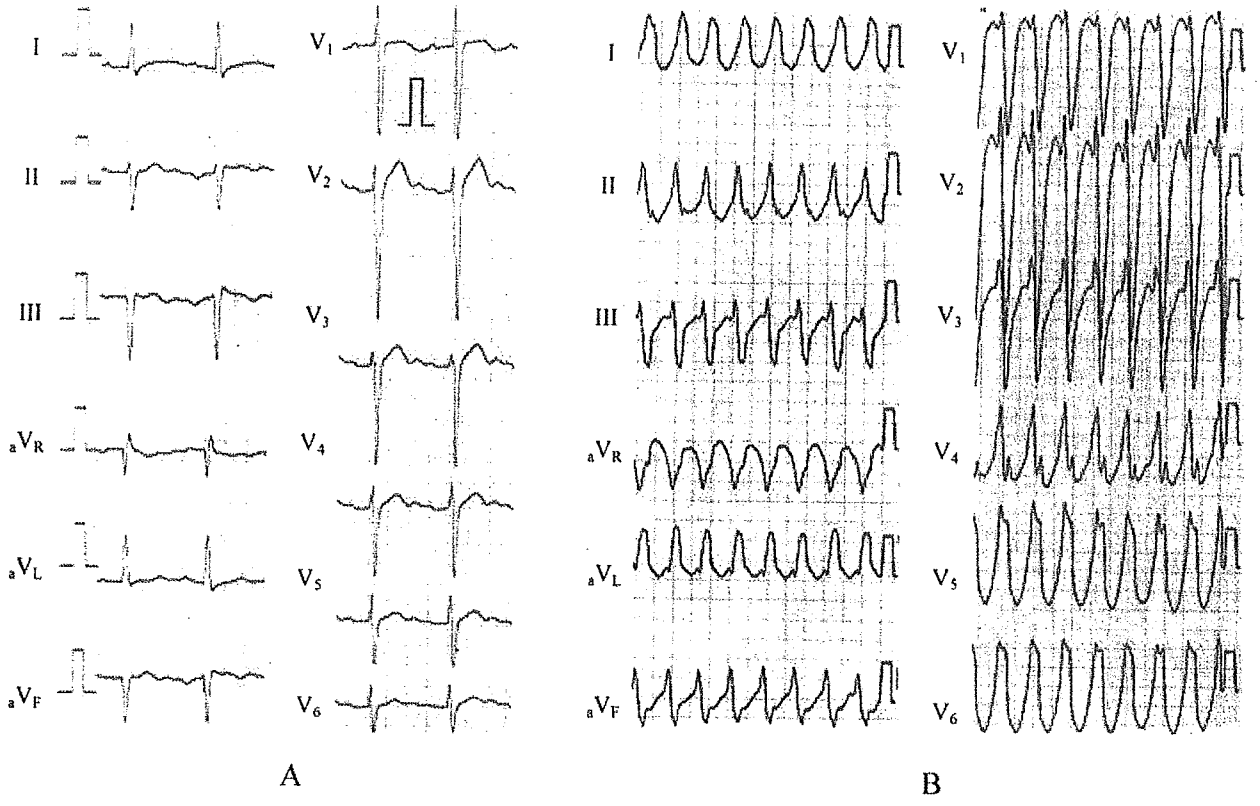

Figure 1. Electrocardiography of this patient at rest (A) and during palpitation attack (B).

muscle and sternocleidomastoid muscle, all of which were characteristic of the DM1 phenotype. Medical Research Council (MRC) scale was 3–4/5 in the upper and lower limbs, and both grip and percussion myotonias were observed. Laboratory data indicated the presence of diabetes mellitus (FBS 172 mg/dl, HbA1c 9.1%). ECG showed PR prolongation, left axis deviation, and clockwise rotation at rest (Fig. 1A) and it revealed that QRS polarity during tachycardia (180 beats/min) was left bundle branch block form with atrioventricular dissociation. Thus, we considered this tachycardia was VT from the right ventricular outflow tract (Fig. 1B). The chest X-ray did not show cardiomegaly, but a coin lesion due to a previously diagnosed calcified epithelial tumor, was detected in the right middle lung field (Fig. 2A, arrow).

The ultrasonic cardiogram (UCG) did not show any abnormal findings (data not shown). Magnetic resonance imaging (MRI) of the heart showed neither dilatation nor diffuse fatty infiltration in the right ventricle (Fig. 2B, C). Cardiac catheterization revealed no abnormality, a mean pulmonary capillary wedge pressure of 5 mmHg and left ventricular pressure of 124/2 mmHg (end-diastolic pressure 7 mmHg). Cardiac index measured by thermodilution method was 3.13 l/min/m^2. Ventriculography showed normal bilateral ventricular wall-motion and cavity size (Fig. 2D–G). No significant stenotic lesions of coronary artery existed (data not shown).

Histological examination of endomyocardial biopsy specimens obtained from the septum near the outflow of the right ventricle showed severe fatty infiltration, increased interstitial fibrosis, atrophy and disarrangement of myocardial cells (Fig. 3A, B). However, biopsy specimens obtained near the apex of the right ventricular septum did not show any change of myocardial cells. Next, an electrophysiological study was performed to examine the mechanism of the ventricular tachycardia. VT was easily induced by a single programmed stimulation from the right ventricular apex (coupling interval 350 msec), but it was not sustained for long (Fig. 4). The QRS wave form during VT induced by single programmed stimulation (Fig. 5) was the same as the clinical VT on 12-lead ECG (Fig. 1B). The local potential which was 32 msec earlier than the onset of QRS during VT was recorded at the septal side of the right ventricular outflow tract (Fig. 6). Precise activation mapping was impossible because of the shortness of VT duration in this session, so we could not detect the site of critical slow conduction, the perfect pace-mapping (Fig. 7) site and the earliest activation site were the targets of catheter ablation and entrainment with concealed fusion was confirmed in the same site. Thus, the mechanism of this VT was considered to be re-entrant. VT was terminated with radiofrequency current application (Max. 40W, and 50°C, respectively) in 12 seconds. (Fig. 8) to the focus,

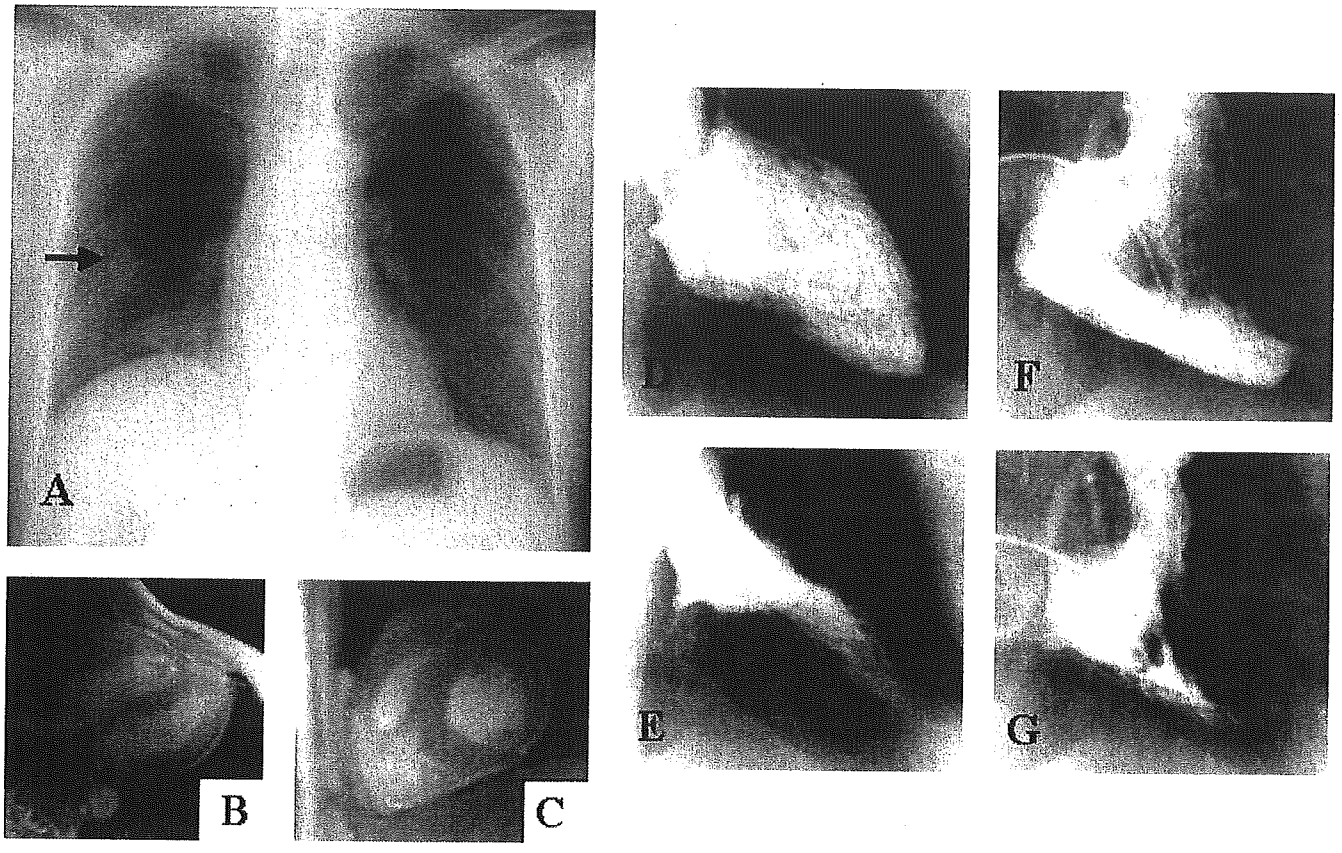

Figure 2. Chest X-ray demonstrated the presence of a coin lesion due to a calcified epithelium tumor in the right middle lung field (arrow), but not cardiomegaly (A). Magnetic resonance imaging of the heart did not show any fatty-fibrosis (B, C). The ventriculogram (left side; D and E, and right side; F and G) showed normal bilateral ventricular wall motion and cavity size. The upper panels indicate the diastolic phase (D and F) and the lower panels indicate the systolic phase (E and G).

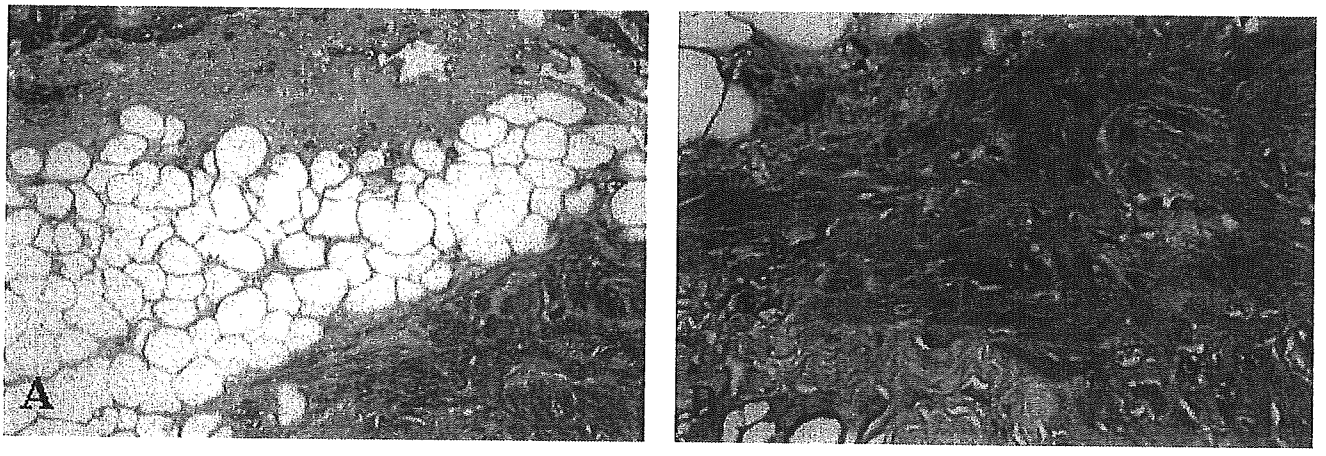

Figure 3. Histological findings of endomyocardial biopsy specimens of the right ventricular septum. Severe fibro-fatty replacement (A) and disarrangement of myocardial cells (B) are observed (A: Azan stain, ×40, B: HE stain, ×100).

that was the same site of endomyocardial biopsy and we have found no recurrence in 2 years.

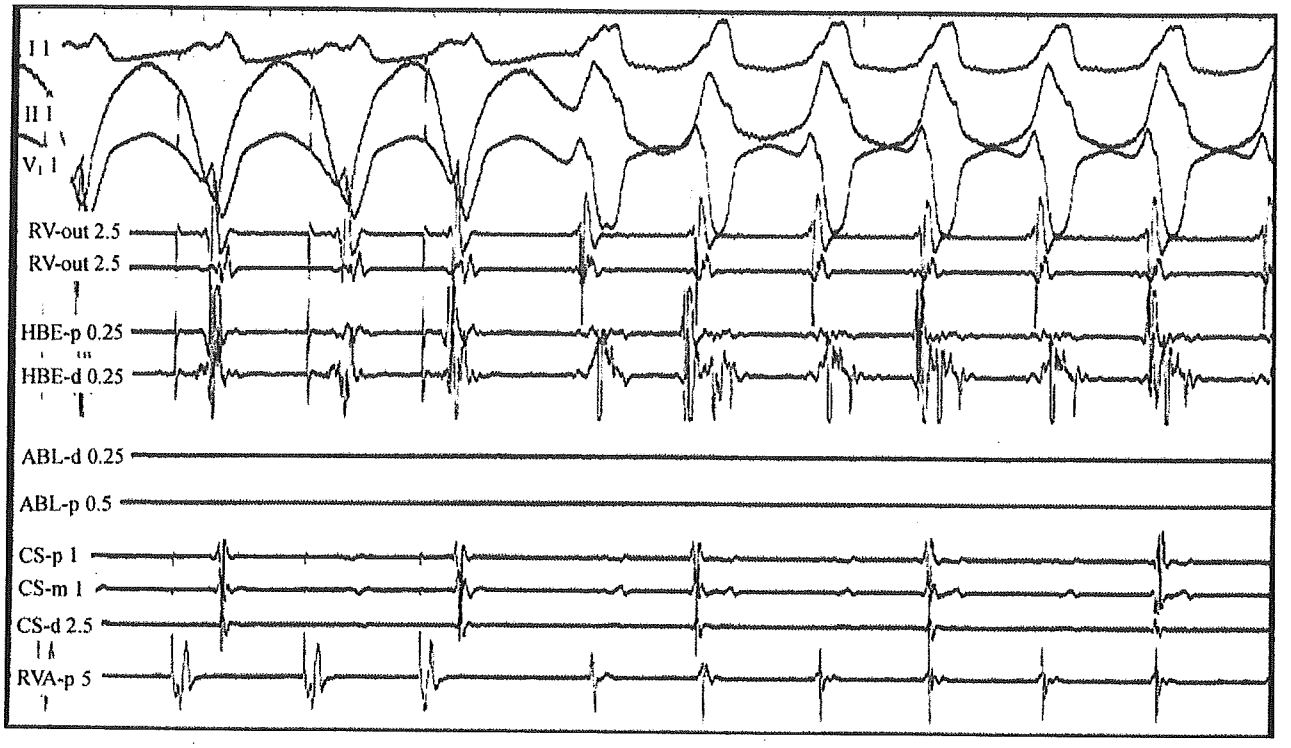

Figure 4. VT induced by single programmed stimulation from the right ventricular apex.

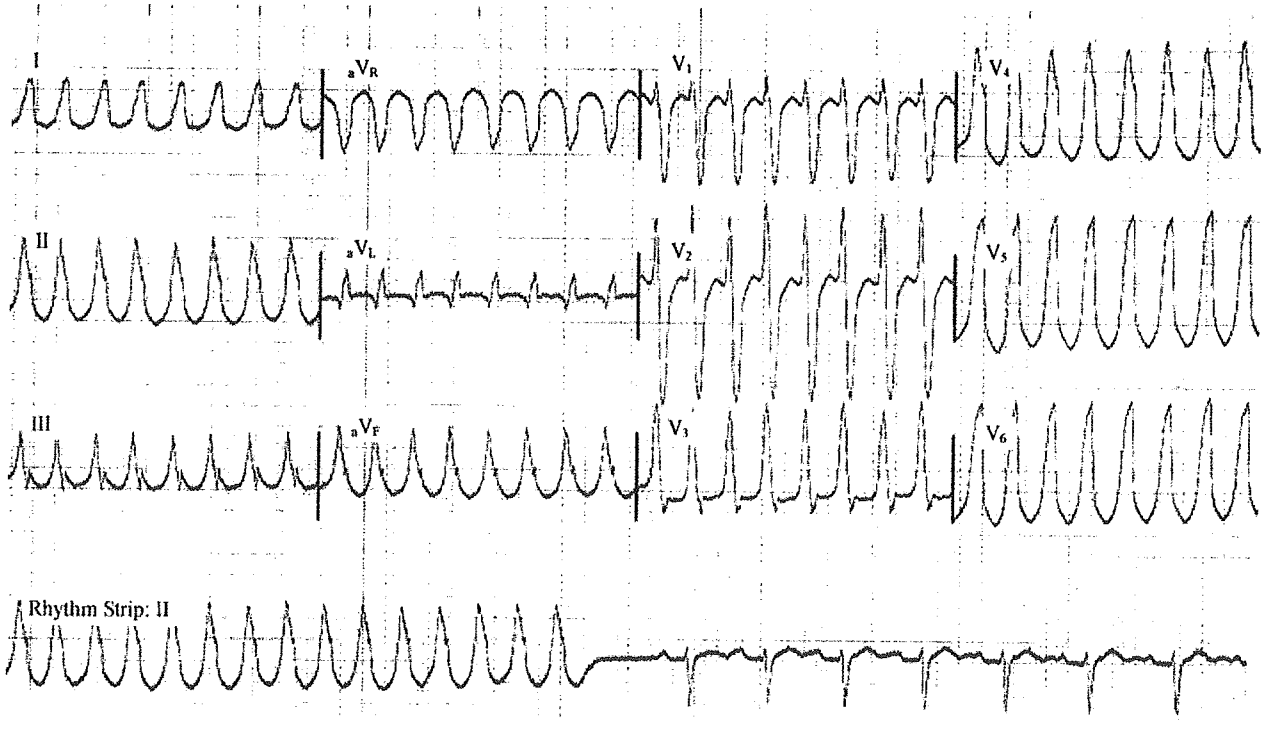

Figure 5. The QRS wave form during VT induced by single programmed stimulation was the same as the clinical VT (Fig. 1B).

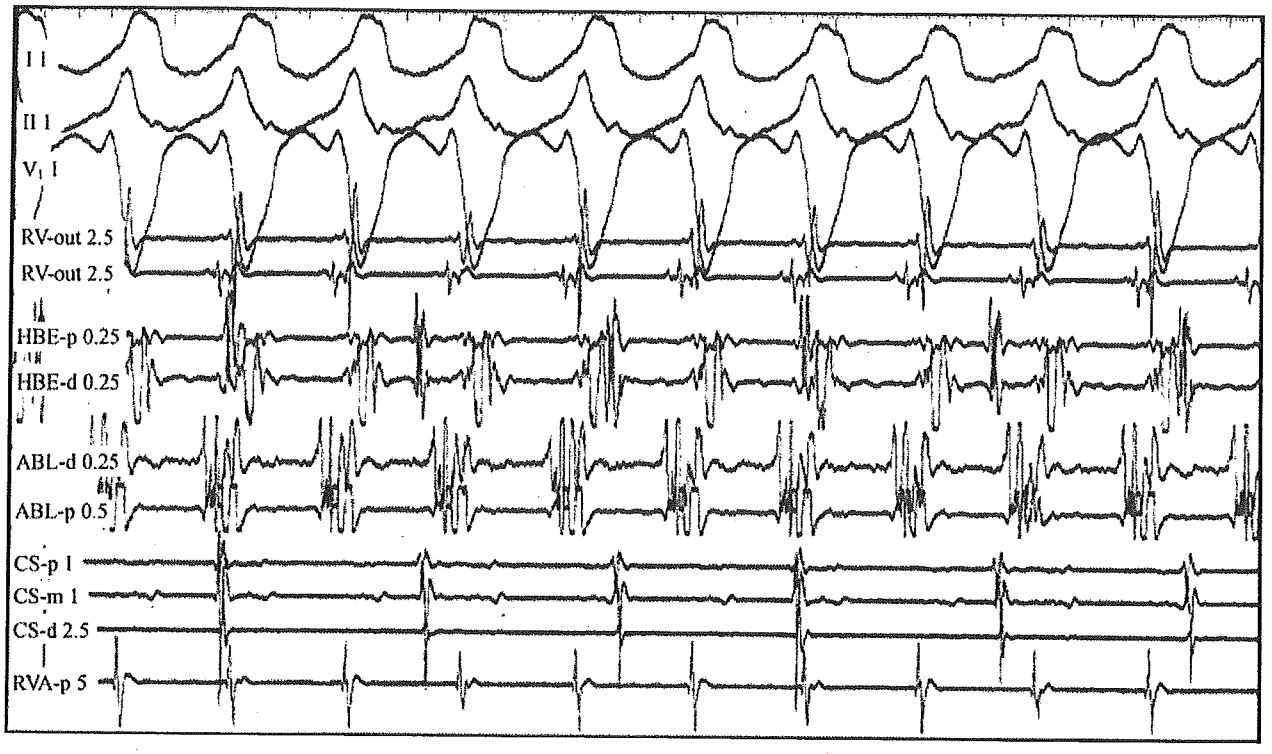

Figure 6. The local potential which was 32 msec earlier than the onset of QRS during VT was recorded at the septal side of the right ventricular outflow tract.

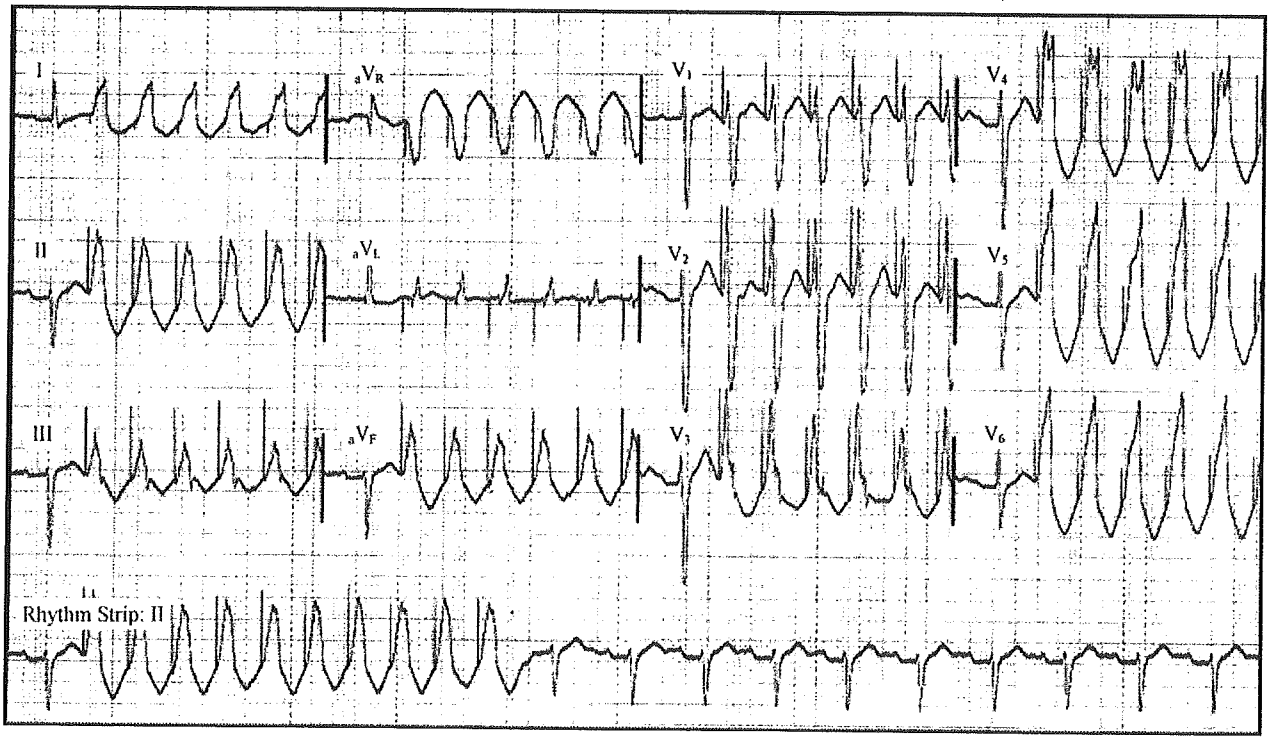

Figure 7. Pace-mapping on 12-lead ECG.

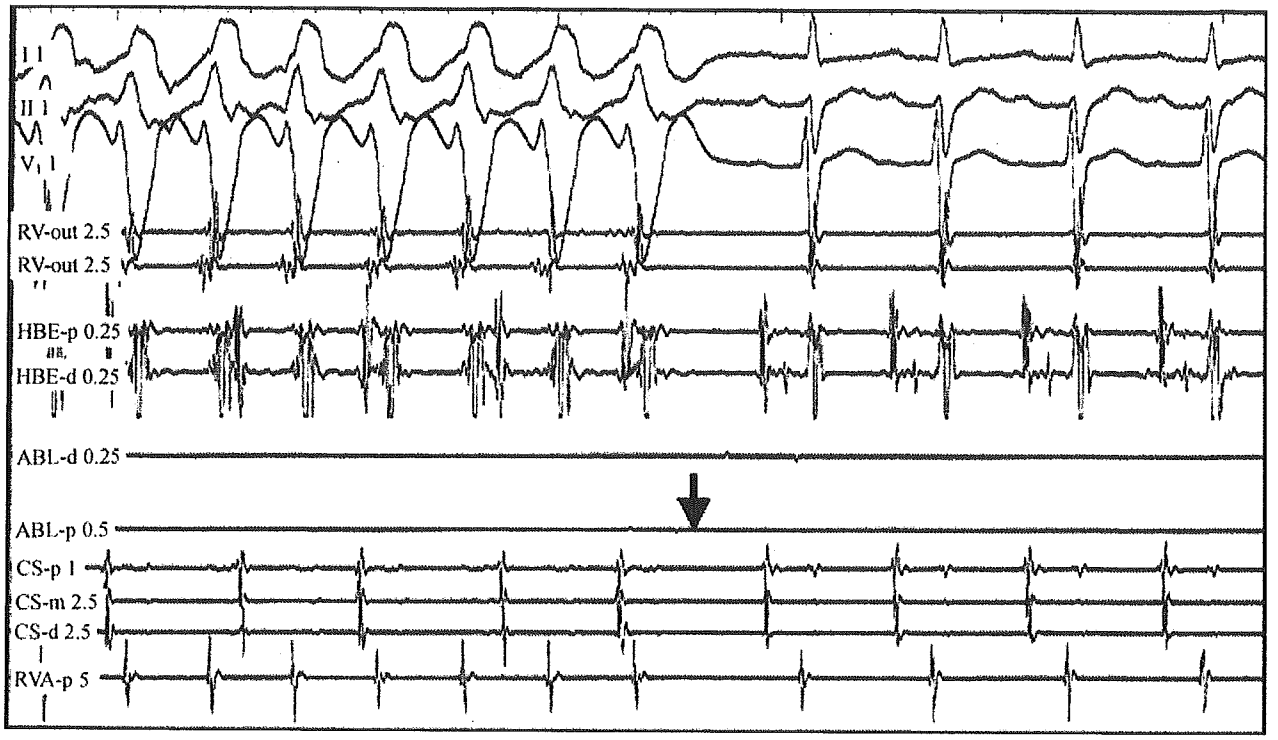

Figure 8. Ventricular tachycardia was terminated by radiofrequency applications (arrow).

Discussion

Conduction disturbance is a well-known cardiac involvement in patients with DM1 because fibrosis and fatty infiltration are often seen in the conduction system (15). Furthermore, histological changes are also seen in the working myocardium (16). Nguyen et al reported that fibrosis of the ventricular myocardium was seen in eleven, fatty infiltration was seen in nine, and cardiomyocyte hypertrophy was seen in seven out of twelve autopsy cases of myotonic dystrophy (15). These results suggest that fatty-fibrosis may become a point of origin of ventricular arrhythmia. Several authors have reported that the mechanism of VT in DM1 might be due to His-Purkinje conduction delay caused by massive fatty fibrosis (11, 13). Additionally, it was recently reported that the focal fatty degeneration of the right ventricle could be demonstrated by MRI in patients with DM1 (17). This suggests that the re-entry circuit could be formed in this site and may become a mechanism of VT. In the present case, UCG, ventriculography, and MRI did not show any dilatation or obvious fatty infiltration of the right ventricle. However, biopsy specimens obtained from the right ventricular septum showed severe fatty infiltration, increased interstitial fibrosis, atrophy and disarrangement of myocardial cells, which appeared to be consistent with DM1. Interestingly, the re-entry circuit was confirmed in the septal side of the right ventricular outflow tract, which coincided with the biopsy site. It was suggested that the re-entry circuit was formed by focal fatty-fibrosis.

The unstable expansion of CTG triplet repeats in the uncoding region of the DMPK-gene is considered to be responsible for the pathological changes associated with this disease (1–5). These changes are not mediated by the DMPK gene itself but by a toxic gain-of-function effect caused by the expanded CTG repeat in the mutant DMPK mRNA. The correlation between CTG-repeat length and the extent of multisystemic disorders in DM1 remains unknown. Some authors have reported that CTG-repeated length correlated well with disease severity in DM, but others have reported that it did not correlate with cataract, myotonia, or cardiac disease (18, 19). In the present patient, a heterozygous and quite long, about 1,800, CTG-repeat expansion in DMPK gene was demonstrated on chromosome 19q13.3. The severity of the DM1-related extra-cardiac events in this patient; atrophy of the zygomatic muscle seemed to correlate well with CTG-repeat expansion as reported in the previous studies.

Regarding cardiac involvement, Tokgozoglu et al reported that myocardial wall motion and abnormalities in the electrocardiogram correlate with CTG-repeat length (20), whereas Lazarus et al reported that impediment of the atrioventricular conducting system does not correlate with CTG-repeat length (21). It remains uncertain whether this patient's cardiac involvement is severe or not; that is the patient has a potentially lethal arrhythmia, and the fatty infiltration was detected by biopsy of the cardiac muscle, but not detected by MRI. All reports concerning the correlation between CTG-

repeat and disease severity were based on the analysis of CTG repeats expansion in each patient's leukocyte rather than in cardiomyocytes. We should focus on CTG repeats in cardiomyocytes when we make an attempt to investigate about the correlation between cardiac involvement and the CTG repeats expansion, as it was recently reported that somatic instability is often seen in patients of DM1 (22, 23).

Implantation of an implantable cardioverter defibrillator (ICD) should be considered to treat VT in patients with DM1, because massive fatty fibrosis in cardiac muscle is often responsible for VT in such cases and several pharmacological treatments have not improved their prognosis. There are several reports of successful catheter ablation against VT in DM1 (13, 24), but, the long-term prognosis has not yet been determined. In the present case, catheter ablation therapy was very useful in reentrant VT (25) and a good long-term prognosis is anticipated, as this case did not show obvious fatty infiltration of the right ventricle on MRI. Catheter ablation resulted in a radical cure of VT, but we should continue to carefully follow this patient carefully for a long period.

References

1) Buxton J, Shelbourne P, Davies J, et al. Detection of an unstable fragment of DNA specific to individuals with myotonic dystrophy. Nature **355**: 547–548, 1992.
2) Harley HG, Brook JD, Rundle SA, et al. Expansion of an unstable DNA region and phenotypic variation in myotonic dystrophy. Nature **355**: 545–546, 1992.
3) Brook JD, McCurrach ME, Harley HG, et al. Molecular basis of myotonic dystrophy: expansion of a trinucleotide (CTG) repeat at the 3'end of a transcript encoding a protein kinase family member. Cell **69**: 385, 1992.
4) Fu Y-H, Pizzuti A, Fenwick RG Jr, et al. An unstable triplet repeat in a gene related to myotonic muscular dystrophy. Science **255**: 1256–1258, 1992.
5) Mahadevan M, Tsilfidis C, Sabourin L, et al. Myotonic dystrophy mutation: an unstable CTG repeat in the 3' untranslated region of the gene. Science **255**: 1253–1255, 1992.
6) Harper PS. Myotonic Dystrophy, 3rd edition. WB Saunders, London, 2000.
7) Church SC. The heart in myotonia atrophica. Arch Intern Med **119**: 176–181, 1967.
8) Fisch C. The heart in dystrophia myotonica. Am Heart J **41**: 525–538, 1950.
9) Motta J, Guilleminault C, Billingham M, Barry W, Mason J. Cardiac abnormalities in myotonic dystrophy: electrophysiologic and histopathologic studies. Am J Med **67**: 467–473, 1979.
10) Cannom DS, Wyman MG, Goldreyer BN. Clinical and induced ventricular tachycardia in a patient with myotonic dystrophy. J Am Coll Cardiol **4**: 625–628, 1984.
11) Grigg LE, Chan W, Mond HG, Vohra JK, Downey WF. Ventricular tachycardia and sudden death in myotonic dystrophy: clinical, electrophysiologic and pathologic features. J Am Coll Cardiol **6**: 254–256, 1985.
12) Hiromasa S, Ikeda T, Kubota K, et al. Ventricular tachycardia and sudden death in myotonic dystrophy. Am Heart J **115**: 914–915, 1988.
13) Merino JL, Carmona JR, Fernandez-Lozano I, Peinado R, Basterra N, Sobrino JA. Mechanisms of sustained ventricular tachycardia in myotonic dystrophy: implications for catheter ablation. Circulation **98**: 541–546, 1998.
14) Stevenson WG, Sweeney MO. Pharmacologic and nonpharmacologic treatment of ventricular arrhythmias in heart failure. Curr Opin Cardiol **12**: 242–250, 1997.
15) Nguyen HH, Wolfe JT III, Holmes DR Jr, Edwards WD. Pathology of the cardiac conduction system in myotonic dystrophy: a study of 12 cases. J Am Coll Cardiol **11**: 662–671, 1988.
16) Phillips MF, Harper PS. Cardiac disease in myotonic dystrophy. Cardiovasc Res **33**: 13–22, 1997.
17) Vignaux O, Lazarus A, Varin J, et al. Right ventricular MR abnormalities in myotonic dystrophy and relationship with intracardiac electrophysiologic test findings: initial results. Radiology **224**: 231–235, 2002.
18) Jaspert A, Fahsold R, Grehl H, Claus D. Myotonic dystrophy: correlation of clinical symptoms with the size of the CTG trinucleotide repeat. J Neurol **242**: 99–104, 1995.
19) Hayashi Y, Ikeda U, Kojo T, et al. Cardiac abnormalities and cytosine-thymine-guanine trinucleotide repeats in myotonic dystrophy. Am Heart J **134**: 292–297, 1997.
20) Tokgozoglu LS, Ashizawa T, Pacifico A, Armstrong RM, Epstein HF, Zoghbi WA. Cardiac involvement in a large kindred with myotonic dystrophy: quantitative assessment and relation to size of CTG repeat expansion. JAMA **274**: 813–819, 1995.
21) Lazarus A, Varin J, Ounnoughene Z, et al. Relationships among electrophysiological findings and clinical status, heart function, and extent of DNA mutation in myotonic dystrophy. Circulation **99**: 1041–1046, 1999.
22) Abbruzzese C, Costanzi Porrini S, Mariani B, et al. Instability of a permutation allele in homozygous patients with myotonic dystrophy type 1. Ann Neurol **52**: 435–441, 2002.
23) Martorell L, Monckton DG, Gamez J, Baiget M. Complex patterns of male germline instability and somatic mosaicism in myotonic dystrophy type 1. Eur J Hum Genet **8**: 423–430, 2000.
24) Shiraishi H, Shirayama T, Inoue K, et al. Successful catheter ablation against ventricular tachycardia associated with myotonic dystrophy. Intern Med **39**: 39–44, 2000.
25) Wen MS, Yeh SJ, Wang CC, Lin FC, Chen IC, Wu D. Radiofrequency ablation therapy in idiopathic left ventricular tachycardia with no obvious structural heart disease. Circulation **89**: 1690–1696, 1994.